RSC Advances

PAPER

View Article Online
View Journal | View Issue

Cite this: *RSC Adv.*, 2017, **7**, 56697

Resistivity and piezoelectric properties of $Ca_3TaGa_{1.5}Al_{1.5}Si_2O_{14}$ single crystals for high temperature sensors†

Xiuwei Fu,*[a] Encarnación G. Víllora,[a] Yoshitaka Matsushita,[a] Yuuki Kitanaka,[b] Yuji Noguchi,[b] Masaru Miyayama,[b] Kiyoshi Shimamura[ac] and Naoki Ohashi[ad]

Received 30th October 2017
Accepted 11th December 2017

DOI: 10.1039/c7ra11926g

rsc.li/rsc-advances

High quality colorless $Ca_3TaGa_{1.5}Al_{1.5}Si_2O_{14}$ (CTGAS) single crystals are successfully grown by the Czochralski method for high temperature (over 200 °C) sensor applications. The full set of properties, including thermal expansion, resistivity, dielectric, elastic and piezoelectric constants, is characterized as a function of temperature for the first time. The thermal expansion of CTGAS is nearly isotropic, which is beneficial to prevent stress and cracking after growth and in various temperature applications. The variation of the dielectric permittivities is about 4% between room temperature and 650 °C, while the dielectric loss is less than 2%. In the same temperature range, the piezoelectric coefficient d_{11} increases from 4.15 to 5.03 pC N^{-1} (about 21%). The average temperature coefficient frequency of the (*XYt*) −30° plate is as small as −15 ppm K^{-1}. Furthermore, the resistivity of CTGAS grown under an low oxygen partial pressure atmosphere is as high as $\sim 4 \times 10^{10}$ Ω cm at 400 °C, which is more than two orders of magnitude better than that of the reference candidate $La_3Ta_{0.5}Ga_{5.1}Al_{0.4}O_{14}$. Altogether, CTGAS exhibits excellent electric and piezoelectric properties at elevated temperatures, and therefore is a promising candidate for high temperature sensor applications.

Introduction

Piezoelectricity was firstly discovered by the Curie brothers in 1880. Since then, it has developed rapidly and now is widely used in modern science and engineering. One of the main applications of piezoelectric materials is sensors due to the high sensitivity, fast response and compactness. In recent years, the field of sensing applications has continued to grow, particularly in those areas involving high temperature (HT).[1–5] For example, a piezoelectric combustion pressure sensor is one relevant case of HT applications.[6] The sensor is installed inside automobile engines for real-time monitoring of the combustion process in order to optimize the combustion efficiency and minimize the formation of environment-harmful gases such as CO_2 and NO_x.

However, the use of piezoelectric materials for HT sensor applications presents many challenges. On the one hand, the most common limitation is the structural instability. For example, the well-known and most widely used lead zirconate titanate (PZT) ceramics undergo a ferroelectric–paraelectric phase transition at relatively low temperatures since their Curie temperatures lie below 350 °C.[1] The α-quartz is the another widely used piezoelectric material that presents excellent piezoelectric properties at room temperature (RT), such as high resistivity, low mechanical loss, narrow bandwidth and excellent thermally piezoelectric stability.[1] Although it is non-ferroelectric, it also has a crystallographic phase transition (at 570 °C), and the maximum temperature for practical applications is even lower due to high electric losses above 450 °C.[7] On the other hand, recently, several materials with relatively good piezoelectric properties have been proposed, however, these present another kind of drawbacks for HT applications. For instance, $GaPO_4$ exhibits a high resistivity and a good thermal stability up to 930 °C, but the growth of single crystals is rather difficult, which seriously limits its potential for commercial applications.[5] On the contrary, rare-earth calcium oxyborate crystals (RECOB) can be easily grown with the Czochralski (Cz) technique and can maintain high resistivity and good piezoelectric properties at HT, however, their pyroelectricity is detrimental for practical sensing applications.[8] Furthermore, AlN has been also considered for HT applications due to its high thermal conductivity and resistivity, as well as excellent dielectric breakdown strength. It turned out, however, that its usage at HT is limited by a poor oxidation resistance.[1,5,9]

[a]*National Institute for Materials Science, Tsukuba 305-0044, Japan. E-mail: fu.xiuwei@nims.go.jp*

[b]*Department of Applied Chemistry, The University of Tokyo, Bunkyo, Tokyo 113-8656, Japan*

[c]*Graduate School of Advanced Science and Engineering, Waseda University, Shinjuku, Tokyo 169-8555, Japan*

[d]*Materials Research Center for Element Strategy, Tokyo Institute of Technology, Midori, Yokohama 226-8503, Japan*

† Electronic supplementary information (ESI) available. See DOI: 10.1039/c7ra11926g

The langasite $La_3Ta_{0.5}Ga_{5.5-x}Al_xO_{14}$ (LTGA, $x = 0$–0.5) single crystal is being considered for HT sensor applications. This compound is characterized by the absence of pyroelectricity and phase transitions up to its melting point (~1500 °C), and a high value of piezoelectric coefficient d_{11} (three times larger than that of α-quartz at RT). Further, it can be grown by the standard Cz technique, so that the production of large-size crystals is feasible.[10,11] However, the structure of LTGA is disordered, which is the cause for a low resistivity at HT (about 10^8 Ω cm at 400 °C).[12] Instead, the resistivity of ordered langasite CTGS single crystal reaches the 10^{10} Ω cm order at 400 °C, *i.e.* about two orders of magnitude better than that of the reference candidate LTGA. It should be noted that a high electrical resistivity is mandatory to minimize losses and to guarantee a reasonable signal/noise ratio.[1] Therefore, the CTGS single crystal is attracting much attention for HT sensors.[13–15] Recently we have shown that the resistivity and piezoelectric coefficient d_{11} of CTGS can be gradually enhanced by the incorporation of Al on the Ga site. We have even succeeded to grow the fully Al-substituted $Ca_3TaAl_3Si_2O_{14}$ (CTAS) crystal, which exhibits the best performance for HT applications.[16] Nevertheless, it was observed that the substitution of Ga by Al favors a structural instability, which manifests as a tendency in CTAS to contain inclusions and to crack.[17,18] A partially substituted crystal is a plausible way to compromise the meritorious growth characteristics of CTGS with the better properties of CTAS. In this sense, it is found that a ratio Ga : Al of 50 : 50, *i.e.* $Ca_3TaGa_{1.5}Al_{1.5}Si_2O_{14}$ (CTGAS), can combine the advantages of both. To date some of the elastic and piezoelectric constants such as s_{11} and d_{11}, have been studied, however, a complete characterization of all of the temperature dependent electro-elastic constants of CTGAS is still missing. Beyond these properties, the electrical resistivity is a key parameter that can be influenced by the growth atmosphere and that needs to be studied in detail.

The purpose of this work is to fully determine the dielectric, elastic and piezoelectric parameters of CTGAS single crystal. For it, CTGAS crystals were grown by the Cz technique. In order to determine the more favorable growth atmosphere for high electrical resistivity, crystals were grown under high and low oxygen partial pressures. The quality of grown crystals was accessed by X-ray rocking curve (XRC) measurements, the thermal expansion by powder X-ray diffraction (XRD), and the electro-elastic properties were investigated by the resonance method as a function of the temperature.

Experimental section

CTGAS single crystals were grown by the Cz technique using a 30 kW RF generator. Commercial oxides powders of 4 N purity, namely $CaCO_3$ (Furuuchi Chemical Co.), Ta_2O_5 (H.C. Starck GmbH), Ga_2O_3 (Kojundo Chemical Laboratory Co., Ltd), Al_2O_3 (Kojundo Chemical Laboratory Co., Ltd) and SiO_2 (Furuuchi Chemical Co.), were weighed stoichiometrically, cold pressed at 300 MPa, and sintered at 1250 °C for 20 hours. Resulting polycrystalline CTGAS ceramics were loaded into Pt crucibles, molten and kept at around its melting point (about 1430 °C) for 10–15 hours before seeding in order to homogenize the melt. Afterwards, two CTGAS single crystals were pulled up using an *a*-oriented CTGS seed, under N_2 + 1% O_2 and air, respectively, in order to study the effect of oxygen partial pressure during growth. It should be noted that oxygen was introduced in both cases to prevent Ga evaporation from melt. The rotation rate and pulling speed were fixed at 12 rpm and 0.5 mm h^{-1}, respectively, from the seeding to final crystal separation.

Single crystal XRD analysis was carried out at RT using a Rigaku VariMax Saturn diffractometer equipped with a Mo Kα radiation ($\lambda = 0.71073$ Å) and CCD detector. A submillimeter-size single crystal was fixed on a thin glass fiber. The collected data were refined and reduced with the Rigaku suite CrystalClear (d*trek program package). The structure was solved using the dual-space algorithm method (SHELXT) and refined by the full-matrix least squares on F^2 using SHELXL-2016/6 in the WinGX program package.[19–21] The XRC measurements were carried out using a PANalytical X'Pert MRD diffractometer equipped with a Cu Kα1 target ($\lambda = 1.54059$ Å) and a hybrid two-bounce Ge (220) monochromator. High-resolution data were recorded on a polished *c*-cut CTGAS plate with a scan step of 0.0001° and 0.5 s integration time. Powder XRD was performed with a Rigaku SmartLab 9 kW diffractometer equipped with a Cu Kα1 radiation and a one-dimensional semiconductor X-ray detector. The diffraction data were collected at RT, then every 100 °C up to 1000 °C, and finally every 50 °C until 1200 °C. The dielectric, elastic and piezoelectric parameters were determined by the resonance method using an Agilent 4294A impedance analyzer. CTGAS belongs to the trigonal system with the space group *P*321, so that there are in total ten independent material parameters: two dielectric permittivities ε_{ij}, two piezoelectric coefficients d_{ij}, and six elastic constants s_{ij}. In order to determine them, the samples were cut based on the IEEE standards

Table 1 Orientation and dimensions of CTGAS samples used for the measurement of dielectric, piezoelectric and elastic constants

Specimens	Dimensions (mm^3)	Vibration mode	Related coefficients
Y-cut plate	5 × 5 × 0.5	—	ε_{11}
Z-cut plate	5 × 5 × 0.5	—	ε_{33}
XY plate	10 × 0.5 × 2	Length extension	d_{11}, s_{11}
YX plate	10 × 0.5 × 2	Thickness/face shear	s_{12}, s_{44}
(*XYt*) +30° plate	10 × 0.5 × 2	Length extension	d_{14}, s_{13}, s_{14}, s_{33}
(*XYt*) +15° plate	10 × 0.5 × 2	Length extension	
(*XYt*) −15° plate	10 × 0.5 × 2	Length extension	
(*XYt*) −30° plate	10 × 0.5 × 2	Length extension	

on piezoelectricity,[22] as shown in detail in Table 1. The electrical resistivity was measured under air using a HIOKI SM8220 Super Megohmmeter. The samples were 10 mm square *Y*-cut plates of 1 mm thickness, with 5 mm square Pt electrodes deposited in the middle of both sides with a Hitachi E-1030 ion sputter.

Results and discussion

Crystal growth

Fig. 1 shows the photographs of the two CTGAS single crystals grown under low and high oxygen partial pressures, namely (a) N_2 + 1% O_2 and (b) air. As can be seen, both crystals are highly transparent and colorless. This contrasts with the typical yellowish coloration observed in crystal grown using Ir crucibles,[23] indicating that the color-related defects have been eliminated. On the other hand, these crystals show a strong faceting character. The facets were determined to be {100} and {001} by the back-reflection Laue technique, in accordance with the habit (schematic of Fig. 1) estimated by the DFDH method,[24,25] using the software Materials Studio.[26]

Crystal structure

The structure data and refinement of CTGAS are listed in Table 2. The corresponding cif file is given in the ESI.† This compound crystallizes in the trigonal system with the space group of *P*321. The unit cell parameters are $a = b = 8.0801$ Å, $c = 4.9553(4)$ Å, $Z = 1$, and $V = 280.18(5)$ Å^3. Fig. 2 shows the crystal structure of CTGAS single crystal projected to (a) ⟨001⟩ and (b) ⟨110⟩ directions. There are four different cationic sites: Ca is located at decahedral site, Ta at the octahedral site, Si at the small tetrahedral site, while Ga and Al occupy randomly another relatively large tetrahedral site. The large Ca ions are in 8 oxygen coordination, with four different Ca–O bond distances resulting from three distinguished oxygen sites. Instead, the large Ta ions are in 6 oxygen coordination, with a single bond distance to one of the oxygen sites. Smaller Ga and Al ions are surrounded by 4 oxygens from two sites, while the Si bond to oxygen in triangular pyramids. From Fig. 2(b), we can see that the large Ca and Ta ions form a two-dimension-layer structure parallel to the

Table 2 Structure data and refinement of CTGAS single crystal

Chemical formula	$Ca_3TaGa_{1.5}Al_{1.5}Si_2O_{14}$
Formula weight (g mol^{-1})	726.42
Temperature (K)	293(2)
Crystal system	Trigonal
Space group	*P*321 (no. 150)
Lattice constants (Å)	$a = b = 8.0801(6)$, $c = 4.9553(4)$
Volume (Å^3)	280.18(5)
Density (g cm^{-3})	4.305
Z	1
F_{000}	339
Absorption coefficient (mm^{-1})	15.129
Crystal size (mm^3)	0.189 × 0.075 × 0.044
Theta range (deg.)	2.91–46.06
Limiting indices	$-16 \le h \le 16$, $-16 \le k \le 16$, $-8 \le l \le 10$
Reflection number	5938
Unique/collected reflection number	1606/1605
R_{int}	0.0406
R/w*R* factors [$I > 2\sigma(I)$]	0.0237/0.0597
R/w*R* factors (all data)	0.0237/0.0597
Goodness of fit	1.212
Largest difference peak/hole (e/Å^3)	4.046/−3.012

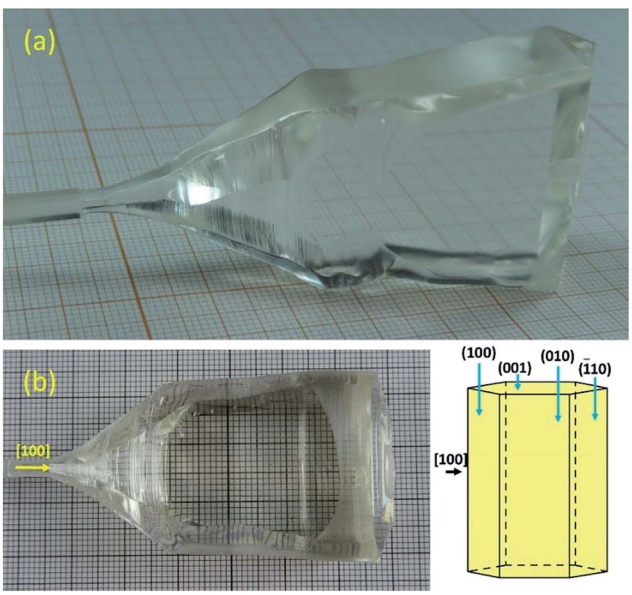

Fig. 1 Photographs of CTGAS single crystals grown under low and high oxygen partial pressures: (a) N_2 + 1% O_2 and (b) air. The expected habit shape based on the DFDH method is shown in the bottom-right schematic.

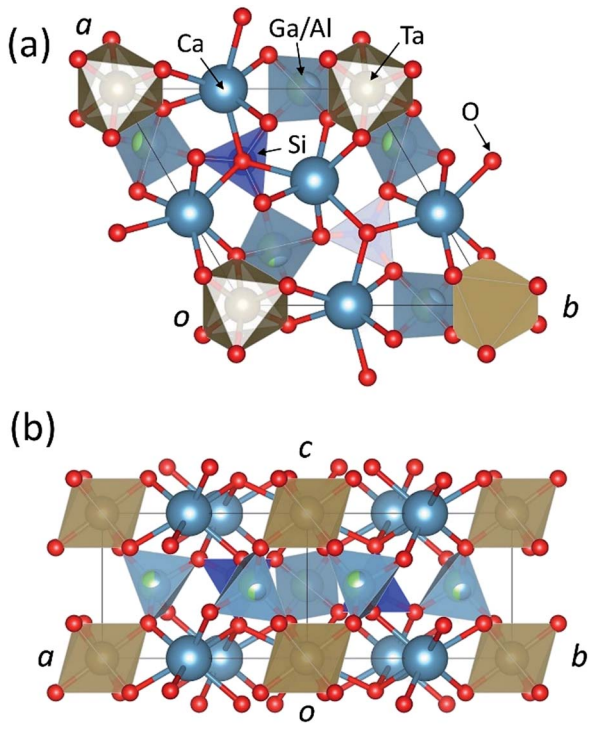

Fig. 2 Crystal structure of CTGAS single crystal projected to: (a) ⟨001⟩ and (b) ⟨110⟩ directions.

c-plane. Similarly, small Al and Si ions form another layer, and both alternate between oxygen layers.

X-ray rocking curve measurement

The XRC of the (002) diffraction peak is shown in Fig. 3. The curve is very symmetric with a full width at half maximum (FWHM) as narrow as 21″, indicating the high crystallinity of grown crystal.

Powder XRD and thermal expansion

Powder XRD patterns were recorded from RT up to 1200 °C. All patterns are similar, with a gradual decrease of 2-theta angles with the increase of temperature due to the lattice expansion. As an example, Fig. 4 shows the good agreement between the measured patterns at 1200 °C and the simulated one from the CTGAS structure at RT. The lack of phase transitions or additional phases up to HT guarantees the stability and viability of CTGAS for HT applications.

The lattice parameters were calculated from the XRD data using the software Fullprof.[27] Fig. 5 shows the lattice constants of CTGAS crystal at RT, together with the reported values for CTGS (Al content, $x = 0$) and CTAS (Al content, $x = 3$).[14,18] The insert illustrates the cation coordination of CTGAS crystal. As can be seen in Fig. 5, the lattice constants decrease linearly with the Al content, in good agreement with the Vegard's law. In addition, the lattice parameters *a*, *c* and cell volume *V* are shown in Fig. 6 as a function of the temperature. All these values increase with temperature due to the thermal expansion. Furthermore, the resulting relative thermal expansion *versus* temperature is fitted with following equations:

$$\Delta a/a_0 = 1.48 \times 10^{-9}T^2 + 6.57 \times 10^{-6}T - 2.58 \times 10^{-4}, \quad (1)$$

$$\Delta c/c_0 = 1.87 \times 10^{-9}T^2 + 6.22 \times 10^{-6}T - 2.10 \times 10^{-4}, \quad (2)$$

where Δa and Δc are the variation of lattice parameters respect to RT, a_0 and c_0 are the lattice parameters at RT, and T is the temperature. For the sake of comparison, the linear thermal expansion coefficients were estimated and are listed in Table 3

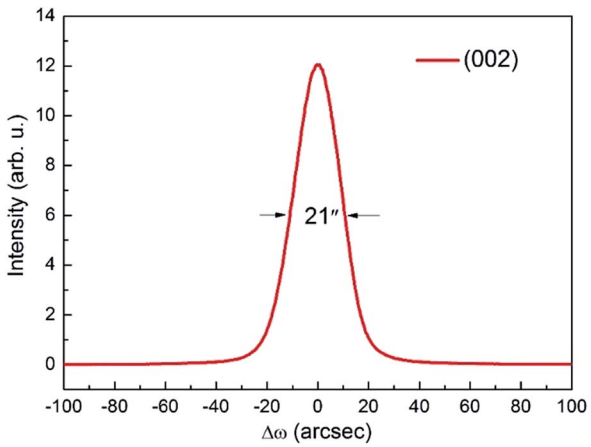

Fig. 3 (002) XRC of CTGAS single crystal.

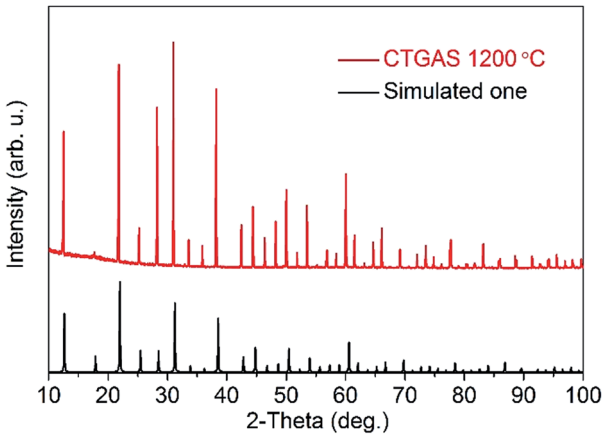

Fig. 4 XRD patterns of CTGAS at 1200 °C, compared with the calculated one at RT.

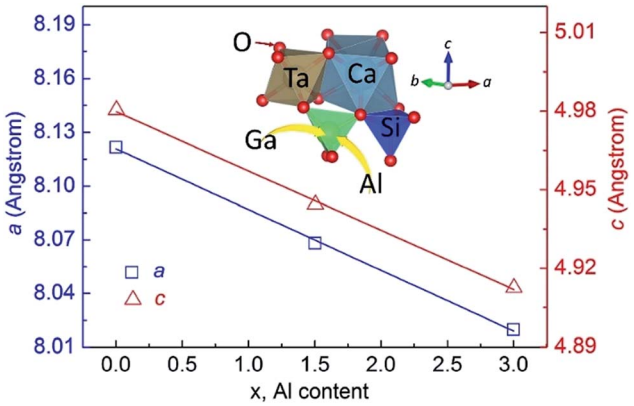

Fig. 5 Lattice constants as a function of Al content at RT. The insert illustrates the coordination of the cations (the errors are smaller than the point size).

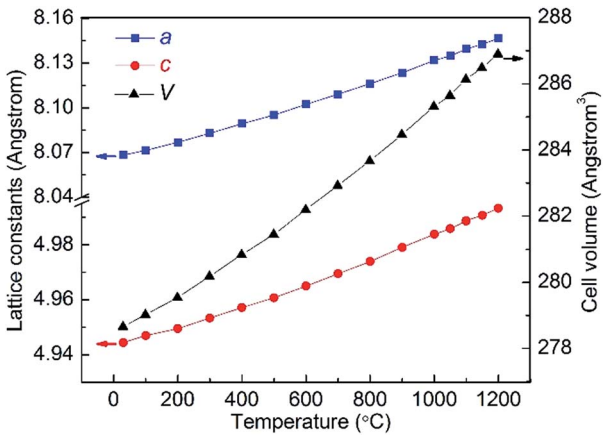

Fig. 6 Lattice constants *a*, *c* and cell volume *V* of CTGAS single crystal as a function of temperature (the errors are smaller than the point size).

together with those of LTGA, CTGS, CTAS and α-quartz crystals.[1,12,14,18] As can be seen, compared to other single crystals, the thermal expansion coefficients of CTGAS along *a*- and *c*-axes are

Table 3 Thermal expansion coefficients of CTGAS single crystal in comparison with LTGA, CTGS, CTAS and α-quartz crystals

Single crystal	*a*-Axis (K^{-1})	*c*-Axis (K^{-1})
LTGA	8.48×10^{-6}	6.32×10^{-6}
CTGS	8.49×10^{-6}	8.17×10^{-6}
CTGAS (this work)	8.44×10^{-6}	8.58×10^{-6}
CTAS	8.51×10^{-6}	9.15×10^{-6}
α-Quartz	13.7×10^{-6}	7.5×10^{-6}

quite close, namely 8.44×10^{-6} and 8.58×10^{-6} K^{-1}, respectively. The similarity of these two values indicates a small anisotropy on thermal expansion, which is beneficial to avoid cracking for HT applications.

Dielectric, elastic and piezoelectric properties

Table 4 lists the RT dielectric, elastic and piezoelectric properties of CTGAS crystal, in comparison with those of CTGS, CTAS and α-quartz crystals. The dielectric permittivities $\varepsilon_{11}^{T}/\varepsilon_0$ and $\varepsilon_{33}^{T}/\varepsilon_0$ at 100 kHz, with values 15.03 and 17.73, respectively, are more than 3 times larger than those of α-quartz. On the other hand, both dielectric parameters decrease with the increase of Al content, in concordance with what can be expected from the Clausius–Mossotti model,[28] which says that the dielectric permittivity increases with the ionic polarizability. The ionic polarizability of Al^{3+} (~0.79 $Å^3$) is about half of that of Ga^{3+} (~1.50 $Å^3$), thus the dielectric permittivity becomes smaller in the order CTGS, CTGAS and CTAS. The elastic compliance constants s_{11}^{E}, s_{12}^{E}, s_{13}^{E}, s_{14}^{E}, s_{33}^{E} and s_{44}^{E} were measured to be 8.80, −3.96, −2.46, −0.16, 5.08 and 22.30, respectively. Apart from s_{14}^{E}, all other constants show same decreasing tendency with Al-substitution as the dielectric permittivities. The piezoelectric coefficients d_{11} and d_{14} are 4.2 and 8.3 pC N^{-1}, respectively, which are about 2 and 11 times larger than those of α-quartz, with values 2.31 and 0.727 pC N^{-1}, respectively. The increase of d_{11} values with Al content may be related to the enhanced lattice distortion with Al substitution.[16]

The dielectric properties measured at 100 kHz as a function of temperature are shown in Fig. 7. As can be seen, both $\varepsilon_{11}^{T}/\varepsilon_0$ and $\varepsilon_{33}^{T}/\varepsilon_0$ present a remarkable thermal stability. The $\varepsilon_{11}^{T}/\varepsilon_0$ exhibits a nearly non-temperature-dependent behavior, showing values around 15 within the measured temperature range. In the case of $\varepsilon_{33}^{T}/\varepsilon_0$, it firstly decreases from 17.73 to 17.00 with a variation of about −4% when temperature increases from RT to 500 °C, and then it almost keeps constant until 650 °C. The up-right insert shows the corresponding dielectric losses, tan δ_{11} and tan δ_{13}, as a function of temperature in comparison with that (tan δ_{11}) of the reference candidate LTGA. It can be seen the dielectric losses of CTGAS are notably low, being even below 2% at temperatures as high as 650 °C. On the contrary, the dielectric losses of LTGA become significant at temperatures above 400 °C.

Fig. 8 shows the variation of the resonance frequency as a function of temperature and the rotation angle for *X*-cut CTGAS samples. In the case of (*XYt*) +30° plate, the resonance frequency could not be measured due the weak

Table 4 Dielectric, elastic and piezoelectric constants of CTGAS crystal at RT in comparison with CTGS, CTAS and α-quartz crystals

	Dielectric permittivities $\varepsilon_{ij}^{T}/\varepsilon_0$ at 100 kHz	
Crystals	$\varepsilon_{11}^{T}/\varepsilon_0$	$\varepsilon_{33}^{T}/\varepsilon_0$
CTGS	16.29	21.62
CTGAS	15.03	17.73
CTAS	13.50	15.30
α-Quartz	4.51	4.63

	Elastic compliance constants s_{ij}^{E} (pm^2 N^{-1})					
	s_{11}^{E}	s_{12}^{E}	s_{13}^{E}	s_{14}^{E}	s_{33}^{E}	s_{44}^{E}
CTGS	9.02	−4.01	−2.88	−0.17	8.13	25.02
CTGAS	8.80	−3.96	−2.46	−0.16	5.08	22.30
CTAS	8.63	−2.90	−2.08	−0.49	4.32	19.09
α-Quartz	12.77	−1.79	−1.22	4.50	9.60	20.04

	Piezoelectric coefficients d_{ij} (pC N^{-1})	
	d_{11}	d_{14}
CTGS	4.0	−14.1
CTGAS	4.2	8.3
CTAS	4.5	5.0
α-Quartz	2.31	0.727

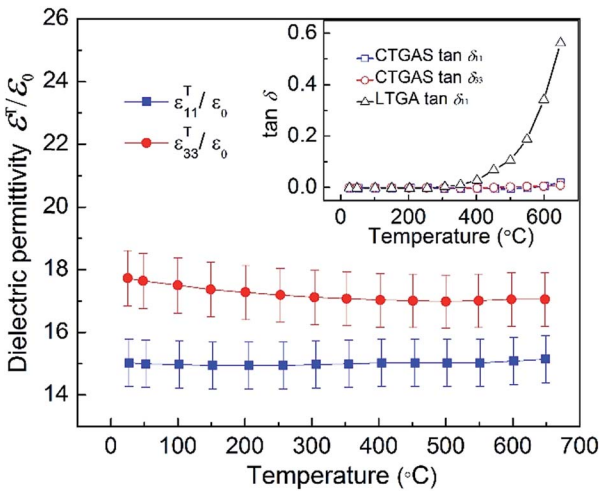

Fig. 7 Dielectric permittivity and tan δ of CTGAS crystal as a function of temperature.

electromechanical effect. The resonance frequency presents a negative dependence for all samples, with the maximum variation being found on the (*XYt*) +15° plate with a temperature coefficient frequency (TCF) of −60 ppm K^{-1} in the range RT-650 °C. Of particular interest is the (*XYt*) −30° plate, which exhibits a high thermal stability and an average TCF of only −15 ppm K^{-1} in the same temperature interval.

The elastic compliance constants *versus* temperature are shown in Fig. 9. As can be seen, all the measured constants increase in the range RT-650 °C: from 8.80 to 9.44, −3.96 to

−4.34, −2.46 to −2.80, −0.16 to −0.47, 5.08 to 5.90 and 22.30 to 22.81 pm^2 N^{-1} for s_{11}^E, s_{12}^E, s_{13}^E, s_{14}^E, s_{33}^E and s_{44}^E, respectively.

Fig. 10 illustrates the piezoelectric coefficients of CTGAS crystal as a function of temperature. The d_{11} increases from 4.15 pC N^{-1} at RT to 5.03 pC N^{-1} at 650 °C with a variation of 21%, while the d_{14}, on the contrary, shows a negative dependence on temperature, decreasing 37% from 8.30 pC N^{-1} at RT to 5.09 pC N^{-1} at 650 °C.

Electrical resistivity

The temperature dependence of the electrical resistivity of CTGAS crystals is shown in Fig. 11 together with the reported for reference LTGA.[12] As can be seen, the resistivity exhibits a linear Arrhenius behavior. It is found that the resistivity of CTGAS depends on the oxygen partial pressure, being higher the lower the oxygen content. At 400 °C it reaches a maximum value of ~4 × 10^{10} Ω cm, which is more than two orders of magnitude higher than that of LTGA reference at the same temperature. On the other hand, the effect of the oxygen partial pressure on activation energy E_a (which determines the slope) is negligible, suggesting that the origin of carriers is the same while its concentration varies. Furthermore, the E_a of CTGAS was calculated to be 1.38 eV, which is larger than that of LTGA with 0.82 eV.

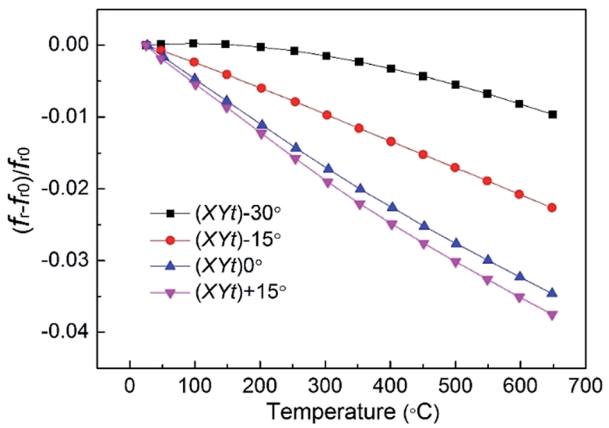

Fig. 8 Variation of the resonance frequency as a function of temperature and rotation angle for *X*-cut CTGAS crystals (the errors are smaller than the point size).

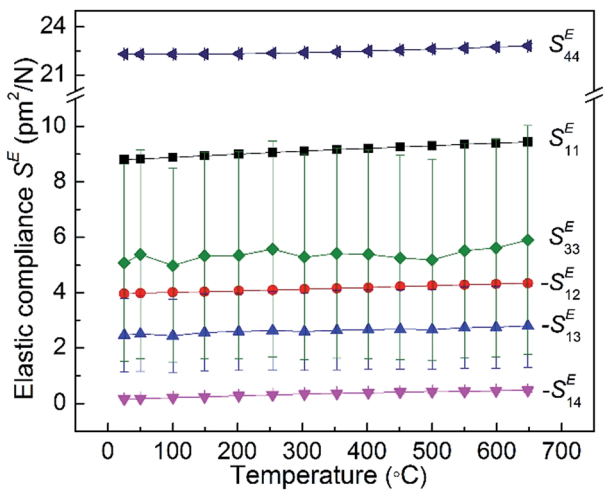

Fig. 9 Elastic compliance constants of CTGAS crystal *versus* temperature.

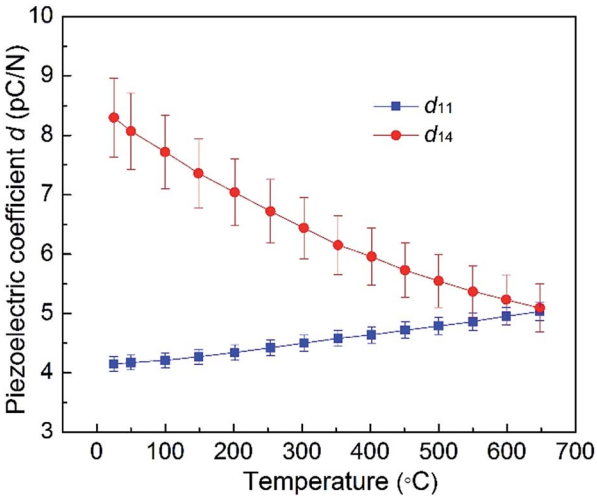

Fig. 10 Piezoelectric coefficients of CTGAS crystal as a function of temperature.

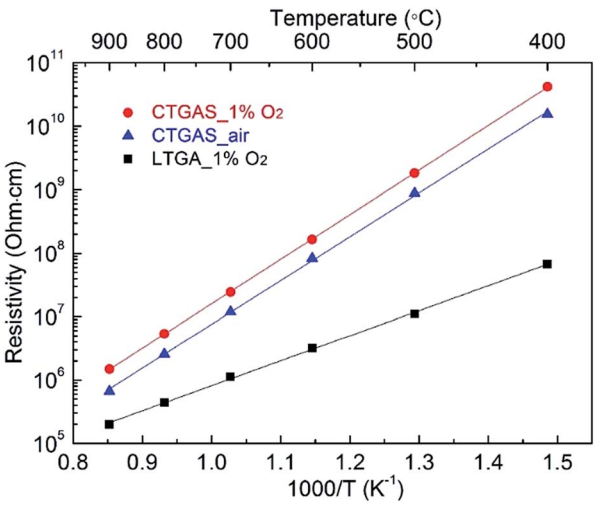

Fig. 11 Temperature dependence of resistivity of CTGAS crystals together with reported LTGA (the errors are smaller than the point size).

Conclusions

Crack- and inclusion-free CTGAS single crystals have been successfully grown by the Cz method under low and high oxygen partial pressures. The crystals were colorless and of high crystalline quality, with a XRC FWHM as narrow as 21 arcsec. XRD analysis indicated that CTGAS did not present neither phase transitions nor second phase segregation up to 1200 °C at

least, and that its thermal expansion was almost isotropic. The dielectric, elastic and piezoelectric constants have been fully investigated as a function of the temperature. The dielectric permittivities of CTGAS showed a high thermal stability, while the dielectric losses were below 2% up to 650 °C. The piezoelectric coefficients d_{11} and d_{14} increase in the same temperature range (RT-650 °C), with values 4.15–5.03 pC N^{-1} and 8.30–5.09 pC N^{-1}, respectively. The crystal grown under the lower oxygen pressure exhibited the highest resistivity. With a value of $\sim 4 \times 10^{10}$ Ω cm at 400 °C, the resistivity of CTGAS is more than two orders of magnitude better than that of LTGA reference. Therefore, CTGAS crystal could be promising for HT piezoelectric sensor applications.

Conflicts of interest

There are no conflicts to declare.

Acknowledgements

This work has been partially supported by the Ministry of Education, Culture, Sports, Science and Technology (MEXT) Element Strategy Initiative to Form Core Center of Japan.

Notes and references

1 S. Zhang and F. Yu, *J. Am. Ceram. Soc.*, 2011, **94**, 3153–3170.
2 C. Shen, H. Zhang, H. Cong, H. Yu, J. Wang and S. Zhang, *J. Appl. Phys.*, 2014, **116**, 044106.
3 C. Shen, S. Zhang, D. Wang, T. Xu, H. Yu, W. Cao, J. Wang and H. Zhang, *CrystEngComm*, 2015, **17**, 1791–1799.
4 F. Yu, Q. Lu, S. Zhang, H. Wang, X. Cheng and X. Zhao, *J. Mater. Chem. C*, 2015, **3**, 329–338.
5 H. Fritze, *J. Electroceram.*, 2011, **26**, 122–161.
6 K. Tsukada, M. Takeuchi, S. Tokumitsu, Y. Ohmura and K. Kawaguchi, *R&D Review of Toyota CRDL*, 1993, **28**, 49–57.
7 R. W. Cernosek, J. R. Bigbie, M. T. Anderson, J. H. Small and P. S. Sawyer, *Presented in part at the Solid-State Sensor and Actuator Workshop*, South Carolina, 1998.
8 F. Yu, F. Chen, S. Hou, H. Wang, Y. Wang, S. Tian, C. Jiang, Y. Li, X. Cheng and X. Zhao, *2016 Symposium on Piezoelectricity, Acoustic Waves, and Device Applications (SPAWDA)*, 2016, pp. 1–7.
9 T. Kim, J. Kim and X. Jiang, *Nondestructive Characterization and Monitoring of Advanced Materials, Aerospace, and Civil Infrastructure*, 2017, vol. 2017, p. 10169, 101691H.
10 I. H. Jung, T. Fukuda and K. H. Auh, *J. Electroceram.*, 2004, **13**, 471–478.
11 H. Takeda, S. Tanaka, H. Shimizu, T. Nishida and T. Shiosaki, *Key Eng. Mater.*, 2006, **320**, 239–242.
12 X. Fu, E. G. Víllora, Y. Oshima, K. Shimamura and N. Ohashi, *J. Alloys Compd.*, 2015, **647**, 1086–1090.
13 F. Yu, X. Zhao, L. Pan, F. Li, D. Yuan and S. Zhang, *J. Phys. D: Appl. Phys.*, 2010, **43**, 165402.
14 X. Fu, E. G. Villora, Y. Matsushita, Y. Kitanaka, Y. Noguchi, M. Miyayama, K. Shimamura and N. Ohashi, *J. Ceram. Soc. Jpn.*, 2016, **124**, 523–527.
15 T. Ma, S. Hou, F. Yu, C. Xie, S. Zhang, J. Wang, J. Du, J. Zhan, X. Cheng and S. Wang, *J. Alloys Compd.*, 2017, **728**, 518–524.
16 X. Fu, E. G. Víllora, Y. Matsushita, Y. Kitanaka, Y. Noguchi, M. Miyayama, K. Shimamura and N. Ohashi, *J. Alloys Compd.*, 2016, **687**, 797–803.
17 J. Xin, Y. Zheng, H. Kong, H. Chen, X. Tu and E. Shi, *Cryst. Growth Des.*, 2008, **8**, 2617–2619.
18 X. Fu, E. G. Villora, Y. Matsushita, Y. Kitanaka, Y. Noguchi, M. Miyayama, K. Shimamura and N. Ohashi, *Cryst. Growth Des.*, 2016, **16**, 2151–2156.
19 L. J. Farrugia, *J. Appl. Crystallogr.*, 1999, **32**, 837–838.
20 G. M. Sheldrick, *Acta Crystallogr., Sect. C: Struct. Chem.*, 2015, **71**, 3–8.
21 G. M. Sheldrick, *Acta Crystallogr., Sect. A: Found. Adv.*, 2015, **71**, 3–8.
22 *IEEE Standard on Piezoelectricity*, ANSI/IEEE Std 176–1987, NY.
23 A. Yoshikawa, Y. Shoji, Y. Ohashi, Y. Yokota, V. I. Chani, M. Kitahara, T. Kudo, K. Kamada, S. Kurosawa and A. Medvedev, *J. Cryst. Growth*, 2016, **452**, 135–140.
24 A. Bravais, *Etudes Crystallographiques*, Academie des Sciences, Paris, 1913.
25 J. D. H. Donnay and D. Harker, *Am. Mineral.*, 1937, **22**, 463.
26 Accelrys, *MS Modeling Getting Started*, Accelrys Software Inc., San Diego, 2006.
27 J. Rodríguez-Carvajal, *Phys. Rev. B: Condens. Matter Mater. Phys.*, 1993, **192**, 55–69.
28 R. D. Shannon, *J. Appl. Phys.*, 1993, **73**, 348–366.